Time reversal symmetry breaking and odd viscosity in active fluids: Green-Kubo and NEMD results (Appendix)

Cory Hargus,[1,*] Katherine Klymko,[2] Jeffrey M. Epstein,[3] and Kranthi K. Mandadapu[1,4,†]

[1] *Department of Chemical and Biomolecular Engineering, University of California, Berkeley, CA, USA*
[2] *Computational Research Division, Lawrence Berkeley National Laboratory, Berkeley, CA, USA*
[3] *Department of Physics, University of California, Berkeley, CA, USA*
[4] *Chemical Sciences Division, Lawrence Berkeley National Laboratory, Berkeley, CA, USA*

I. Simulation Details [1]

To investigate the viscous behavior of a fluid composed of self-spinning dumbbells, we perform molecular dynamics simulations in LAMMPS [1], implementing our own modifications [2] to impose microscopic driving forces and compute the active stress $\boldsymbol{T}^{\mathrm{A}}$. All measured quantities in both the Green-Kubo and NEMD calculations are converged with respect to timestep and system size.

Particles interact with their non-bonded neighbors through a Weeks-Chandler-Andersen [2] potential defined by

$$V_{ij}^{\mathrm{WCA}}(r) = \begin{cases} 4\epsilon\left[\left(\sigma/r\right)^{12} - \left(\sigma/r\right)^{6}\right] + \epsilon & r < 2^{1/6}\sigma \\ 0 & r \geq 2^{1/6}\sigma\,. \end{cases} \tag{A.1}$$

Here, σ, ϵ and particle mass m are the characteristic length, energy, and mass scales, which are used to define the Lennard-Jones units system. All numerical settings and results in this Communication are reported in Lennard-Jones units. The two particles in a single dumbbell are held together by a harmonic potential $V(r) = \frac{1}{2}k(r - r_0)^2$ with spring constant $k = 100$ and reference length $r_0 = 1$.

Dynamics are evolved according to underdamped Langevin dynamics (23) with bath temperature $T = 1.0$ and friction $\zeta = 2.0$. We apply the Langevin bath interactions only along the x_2 direction, so as not to impede flow in the x_1 direction, and employ these conditions in both Green-Kubo and periodic Poiseuille simulations. We note that imposing bath interactions selectively along x_2 may lead to a violation of isotropy by aligning dumbbells along a preferred axis. In all simulations, however, we check that dumbbells have no preferred alignment by measuring the departure of the bond angle of a dumbbell projected onto $[0, \pi/2]$ from the reference value of $\pi/4$:

$$\delta\theta_i^+ = \arctan\left(\frac{|\mathbf{d}_i \cdot \mathbf{e}_2|}{|\mathbf{d}_i \cdot \mathbf{e}_1|}\right) - \frac{\pi}{4}\,. \tag{A.2}$$

We find that in all simulations, $\max(|\langle\delta\theta_i^+\rangle|) < 0.01$ radians, where angle brackets indicate averaging in time and maximization is in space. We also confirm that the density is indeed uniform in all periodic Poiseuille calculations. The relative spatial variation in the density is bounded in all simulations by $\left(\langle(\delta\rho)^2\rangle/\langle\rho^2\rangle\right)^{1/2} < 0.1\%$.

II. Green-Kubo Formula for Shear Viscosity

We also perform a derivation to obtain separate expressions for the shear and bulk viscosities. To this end, we begin with the following equation (also equation (127) in the SI of [3] in the absence of internal spin):

$$k^j k^l \eta_{ijkl} = \frac{1}{\rho_0 \mu} k^j k^l \int_0^\infty dt\ \langle \delta T_{\mathbf{k}}^{ij}(t) \delta T_{-\mathbf{k}}^{kl}(0)\rangle = \frac{1}{\rho_0 \mu} k^j k^l \mathcal{T}_{ijkl}^{\mathbf{k}}\,, \tag{A.3}$$

---

[1] Note that all equations and figures appearing in this appendix are indexed with the prefix "A". References without an "A" refer to the main text.

[2] We have published our simulation and analysis code at https://github.com/mandadapu-group/active-matter.

where

$$\mathcal{T}^{\mathbf{k}}_{ijkl} = \int_0^\infty dt\ \langle \delta T^{ij}_{\mathbf{k}}(t)\delta T^{kl}_{-\mathbf{k}}(0)\rangle\,. \tag{A.4}$$

Following [3], we can obtain an equation for λ_1 and λ_2

$$\lambda_1 + 2\lambda_2 = \frac{1}{2\rho_0\mu}\delta_{ik}\delta_{jk}\mathcal{T}^{\mathbf{k}}_{ijkl}\,, \tag{A.5}$$

in the limit of $\mathbf{k}\to\mathbf{0}$.

To separate λ_1 from λ_2 we return to (A.3) and contract both sides with $k^i k^k$ to obtain

$$k^i k^j k^k k^l \eta_{ijkl} = \frac{1}{\rho_0\mu}k^i k^j k^k k^l \mathcal{T}^{\mathbf{k}}_{ijkl}\,. \tag{A.6}$$

The resulting equation holds independently for any choice of $\mathbf{k}$ in the limit $\mathbf{k}\to 0$. Now, we set $\mathbf{k} = k(\mathbf{e}_1+\mathbf{e}_2)$ and $\mathbf{k} = k(\mathbf{e}_1-\mathbf{e}_2)$ in (A.6) and sum the resulting equations to obtain

$$4\lambda_1 + 4\lambda_2 = \frac{1}{\rho_0\mu}\left(\mathcal{T}^{\mathbf{k}}_{1111}+\mathcal{T}^{\mathbf{k}}_{1122}+\mathcal{T}^{\mathbf{k}}_{1212}+\mathcal{T}^{\mathbf{k}}_{1221}+\mathcal{T}^{\mathbf{k}}_{2112}+\mathcal{T}^{\mathbf{k}}_{2121}+\mathcal{T}^{\mathbf{k}}_{2211}+\mathcal{T}^{\mathbf{k}}_{2222}\right), \tag{A.7}$$

which cannot be written in compact form as a contraction of Kronecker and Levi-Civita tensors with $\mathcal{T}^{\mathbf{k}}_{ijkl}$. Subtracting (A.7) from twice (A.5) and invoking the symmetry of the stress fluctuations gives

$$\begin{aligned}\lambda_2 &= \frac{1}{4\rho_0\mu}(\mathcal{T}^{\mathbf{k}}_{1111}-\mathcal{T}^{\mathbf{k}}_{1122}-\mathcal{T}^{\mathbf{k}}_{2211}+\mathcal{T}^{\mathbf{k}}_{2222}+\mathcal{T}^{\mathbf{k}}_{1212}-\mathcal{T}^{\mathbf{k}}_{1221}-\mathcal{T}^{\mathbf{k}}_{2112}+\mathcal{T}^{\mathbf{k}}_{2121})\\ &= \frac{1}{4\rho_0\mu}(\mathcal{T}^{\mathbf{k}}_{1111}-\mathcal{T}^{\mathbf{k}}_{1122}-\mathcal{T}^{\mathbf{k}}_{2211}+\mathcal{T}^{\mathbf{k}}_{2222})\,.\end{aligned} \tag{A.8}$$

Finally, returning to the definition of $\mathcal{T}^{\mathbf{k}}_{ijkl}$ in (A.3), and taking the zero wavevector limit $\mathbf{k}\to 0$ yields

$$\begin{aligned}\lambda_2 &= \frac{1}{4\rho_0\mu}\int_0^\infty dt\ \langle(\delta T_{22}(t)-\delta T_{11}(t))(\delta T_{22}(0)-\delta T_{11}(0))\rangle\\ &= \frac{1}{\rho_0\mu}\int_0^\infty dt\ \langle\delta T_{12}(t)\delta T_{12}(0)\rangle\,,\end{aligned} \tag{A.9}$$

where, in obtaining the last equality, we use material isotropy to make the stress transformation $\boldsymbol{T'} = \boldsymbol{R^T T R}$ corresponding to a two-dimensional rotation $\boldsymbol{R}$ of angle $\pi/4$, for which $T'_{12} = \frac{1}{2}(T_{22}-T_{11})$. The last equality in (A.9) is the standard Green-Kubo relation for the shear viscosity. One may evaluate either of these expressions to compute the shear viscosity λ_2.

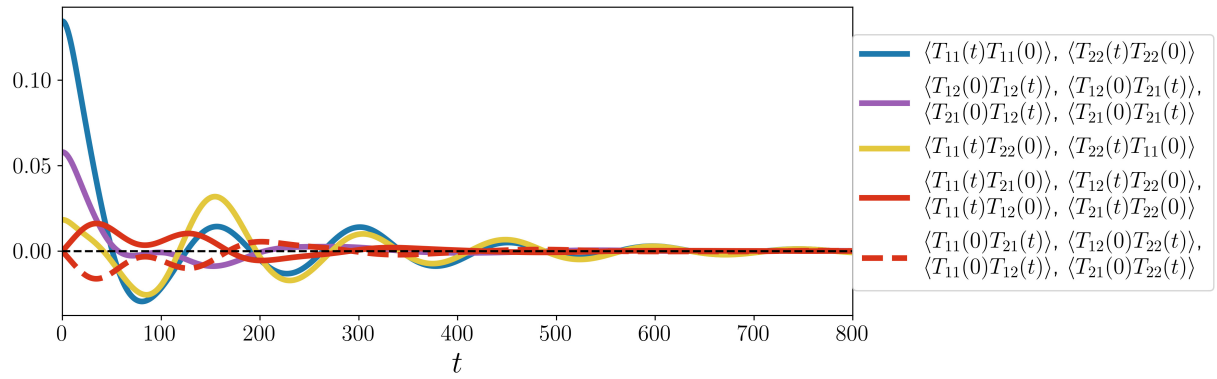

FIG. A.1. The sixteen stress correlation functions computed at $\rho_0 = 0.4$, Pe = 12. Due to symmetries present in the chiral active dumbbell model, many of the correlation functions are identical, and are grouped as such. From this grouping, it is possible to ascertain that certain viscosity coefficients defined in (8)-(13) will vanish. For example, λ_3 depends on a sum of the correlation functions $\mathcal{T}_{1212}-\mathcal{T}_{1221}-\mathcal{T}_{2112}+\mathcal{T}_{2121}$. Here we see that these four correlation functions are identical, hence their sum will be zero. We further observe that the correlation functions contributing to the odd viscosity λ_4 go to zero in the static limit $t\to 0$, a consequence of the antisymmetry identified in (33).

III. Decomposed contributions to the viscosity coefficients from the Irving-Kirkwood stress tensor

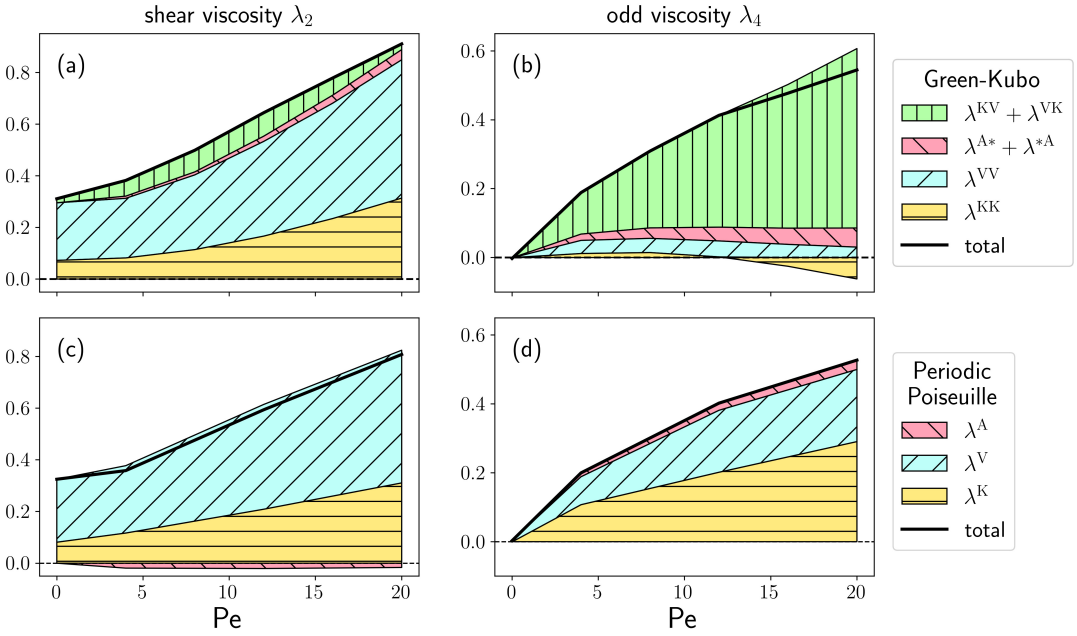

FIG. A.2. Components of the stress contributing to Green-Kubo and Poiseuille calculations of the shear and odd viscosity at $\rho_0 = 0.4$ as a function of Pe. Figures (a) and (b) are the component-wise contributions to λ_2 and λ_4, respectively, from Green-Kubo calculations according to the decompositions in (A.10) and (A.11). Here, $\lambda^{A*} + \lambda^{*A} = \lambda^{AK} + \lambda^{AV} + \lambda^{KA} + \lambda^{VA} + \lambda^{AA}$. Figures (c) and (d) are the component-wise contributions to the λ_2 and λ_4, respectively, in periodic Poiseuille calculations. The solid black line indicates the total viscosity coefficient, obtained by adding the shaded areas above $y = 0$ and subtracting those below $y = 0$.

The Irving-Kirkwood procedure provides a natural decomposition of the stress tensor into kinetic, virial, and active molecular contributions (24). In Fig. A.2, we examine the component-wise stress contributions to the shear and odd viscosity in both Green-Kubo and periodic Poiseuille calculations. The stress appears twice in the correlation functions entering the Green-Kubo equations *via* (14), thus there are nine components contributing to the Green-Kubo viscosity coefficients, which we label λ^{KK}, λ^{KV}, λ^{KA}, λ^{VK}, λ^{VV}, λ^{VA}, λ^{AK}, λ^{AV} and λ^{AA}.

From (22), we define a decomposed shear viscosity as

$$\lambda_2^{XY} = \frac{1}{\rho_0 \mu} \int_0^\infty dt \, \langle \delta T_{12}^X(t) \delta T_{12}^Y(0) \rangle \,, \tag{A.10}$$

where $X, Y \in \{\mathrm{K}, \mathrm{V}, \mathrm{A}\}$ indicate the kinetic, virial and active parts. Similarly, the odd viscosity from (21) may be decomposed as

$$\lambda_4^{XY} = \frac{1}{4\rho_0 \mu} \int_0^\infty dt \, \langle \delta T_{ij}^X(t) \delta T_{kl}^Y(0) \rangle \epsilon_{ik} \delta_{jl} \,. \tag{A.11}$$

For periodic Poiseuille calculations, the decompositions contributing to the viscous coefficients simply involve the choice of whether to use $\boldsymbol{T}^{\mathrm{K}}$, $\boldsymbol{T}^{\mathrm{V}}$, or $\boldsymbol{T}^{\mathrm{A}}$ in (36) and (37), corresponding to λ^{K}, λ^{V}, and λ^{A}, respectively. We observe that the active stress $\boldsymbol{T}^{\mathrm{A}}$ plays a small but not insignificant role in both λ_2 and λ_4 at $\mathrm{Pe} \neq 0$. Notably, the dominant Green-Kubo contributions to λ_2 are λ^{KK} and λ^{VV} while the cross correlations λ^{KV} and λ^{VK} are dominant in λ_4.

IV. Periodic Poiseuille Simulation

Non-equilibrium molecular dynamics simulations allow measurement of viscosity coefficients in direct analogy to experimental viscometry. For the chiral active dumbbell fluid, $\gamma_1 = \gamma_2 = \lambda_3 = \lambda_5 = \lambda_6 = 0$, resulting in decoupling

of the linear and angular momentum balances and leading to modified Navier-Stokes equations

$$\rho \dot{v}_i = \lambda_1 v_{k,ki} + \lambda_2 v_{i,jj} + \lambda_4 \epsilon_{ik} v_{k,jj} - p_{,i} + \epsilon_{ij} p^*_{,j} + \rho g_i \,, \tag{A.12}$$

with bulk viscosity λ_1, shear viscosity λ_2, odd viscosity λ_4, pressure p, and body force g_i.

In the periodic Poiseuille simulations, we subject the system to equal and opposite body forces in the x_1 direction across a rectangular channel of width $2L$, as depicted in Fig. 3. In general, the non-uniform normal stress $\Delta T_{11}(x_2)$, due to the odd viscosity, may cause compression and extension of the fluid such that the steady state density is non-uniform in the x_2 direction. Accordingly, we ensure that the body force g_1 driving the flow is sufficiently small in all simulations so that the density ρ is well-approximated as constant, as described in Appendix I. Therefore, we consider a steady state exhibiting incompressible flow, *i.e.,*

$$v_{i,i} = 0 \,, \tag{A.13}$$

and obtain the simplified constitutive and Navier-Stokes equations:

$$T_{ij} = \lambda_2 \big(v_{i,j} + v_{j,i}\big) + \lambda_4 \big(\epsilon_{ik} v_{k,j} + \epsilon_{jk} v_{i,k}\big) - p\delta_{ij} + p^* \epsilon_{ij} \,, \tag{A.14}$$

and

$$\rho_0 v_{i,j} v_j = \lambda_2 v_{i,jj} + \lambda_4 \epsilon_{ik} v_{k,jj} - p_{,i} + \epsilon_{ij} p^*_{,j} + \rho_0 g_i \,. \tag{A.15}$$

where ρ_0 is the uniform reference density.

We now seek a steady state analytical solution for the velocity and pressure profiles of a fluid between two plates separated by a distance L, subjected to a body force $\mathbf{g} = (g_1, 0)$, where g_1 is uniform in space. The solution is analogous to that of a planar Poiseuille flow, with boundary conditions $v_i = 0$ at $x_2 = 0$ and $x_2 = L$. Using the ansatz $v_1 = v_1(x_2)$, $v_2 = 0$, $p = p(x_2)$, and $p^* = \text{const}$, conditions which are observed in all non-equilibrium simulations considered in this study, one may find the steady state solution to be

$$v_1(x_2) = \frac{\rho_0 g_1}{2\lambda_2} x_2 (L - x_2) \,, \tag{A.16}$$

and

$$p(x_2) = \frac{\lambda_4}{\lambda_2} \rho_0 g_1 x_2 + p_0 \,, \tag{A.17}$$

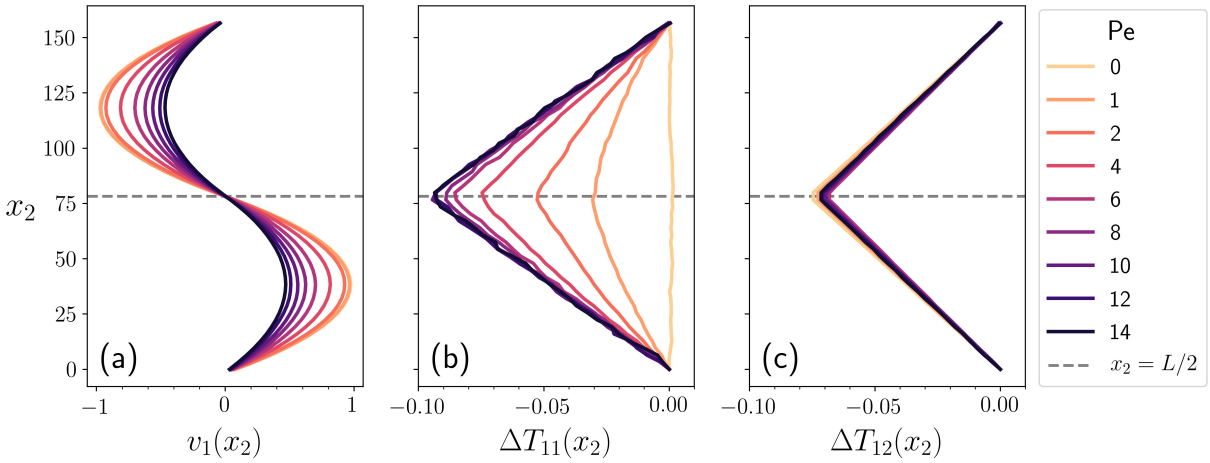

FIG. A.3. Time-averaged velocity and stress profiles from periodic Poiseuille simulations at $\rho_0 = 0.4$ over a range of Pe. Axes are chosen to be consistent with the schematic in Fig. 3. Figure (a) shows the velocity profile $v_1(x_2)$, where the increase in shear viscosity with increasing Pe is apparent, as described in (A.18), in the decrease of the average velocity with increasing Pe. Figures (b) and (c) show $\Delta T_{11}(x_2) = T_{11}(x_2) - \Delta T_{11}(0)$ and $\Delta T_{12}(x_2) = T_{12}(x_2) - \Delta T_{12}(0)$, respectively. Spatial variation in T_{11} is seen to arise due to odd viscosity at Pe $\neq 0$ as in (A.22), while the slope of T_{12} is unaffected by Pe, supporting the ansatz of constant p^* used in (A.16) and (A.17).

where p_0 is an arbitrary reference pressure.

We see that the steady state velocity profile is identical to the usual solution for planar Poiseuille flow, remaining unaffected by odd viscosity. In fact it is always true that odd viscosity does not appear in the velocity profile in incompressible flows with no-slip boundary conditions [4]. The odd viscosity does appear, however, in a pressure gradient arising in the x_2-direction to maintain the no-penetration condition at the walls, *i.e.* to prevent flow in the x_2-direction. Our active dumbbell fluid simulations show parabolic velocity profiles consistent with (A.16) and (A.17) when subjected to equal and opposite body forces as shown in Fig. 3.

Integrating the velocity profile to get an average velocity $\bar{v} = \frac{1}{L}\int_0^L v_1(x_2)dx_2$, we obtain a convenient expression for computing the shear viscosity λ_2 in molecular simulations:

$$\lambda_2 = \frac{\rho_0 g_1 L^2}{12\bar{v}}\,. \tag{A.18}$$

As noted above, λ_4 does not appear in the velocity but in the stress (A.14). For the velocity profile (A.16),

$$T_{11} = -p + \lambda_4 v_{1,2}\,, \tag{A.19}$$

which results in

$$T_{11,2} = -p_{,2} + \lambda_4 v_{1,22}\,. \tag{A.20}$$

Using (A.15) in the x_2-direction, one may reduce (A.20) to

$$T_{11,2} = 2\lambda_4 v_{1,22} = -2\lambda_4 \frac{\rho_0 g_1}{\lambda_2}\,. \tag{A.21}$$

Finally, rearranging (A.21), λ_4 is obtained in terms of the slope of T_{11} as

$$\lambda_4 = \frac{T_{11,2}}{2v_{1,22}} = -\frac{\lambda_2 T_{11,2}}{2\rho_0 g_1}\,. \tag{A.22}$$

where T_{11} can be calculated using the Irving-Kirkwood formula (24) for the active dumbbell fluid.

* hargus@berkeley.edu
† kranthi@berkeley.edu

[1] S. J. Plimpton, J. Comp. Phys. **117**, 1 (1995), see also http://lammps.sandia.gov/.
[2] J. D. Weeks, D. Chandler, and H. C. Andersen, The journal of chemical physics **54**, 5237 (1971).
[3] J. M. Epstein and K. K. Mandadapu, arXiv:1907.10041 (2019).
[4] S. Ganeshan and A. G. Abanov, Physical review fluids **2**, 094101 (2017).